Hindawi
Mathematical Problems in Engineering
Volume 2019, Article ID 4842102, 12 pages
https://doi.org/10.1155/2019/4842102

Research Article

Detection and Extraction of Weak Pulse Signals in Chaotic Noise with PTAR and DLTAR Models

Liyun Su, Li Deng, Wanlin Zhu, and Shengli Zhao

School of Science, Chongqing University of Technology, Chongqing 400054, China

Correspondence should be addressed to Liyun Su; cloudhopping@163.com

Received 29 May 2019; Revised 4 August 2019; Accepted 10 August 2019; Published 28 August 2019

Academic Editor: Javier Martinez Torres

With the development in communications, the weak pulse signal is submerged in chaotic noise, which is very common in seismic monitoring and detection of ocean clutter targets, and is very difficult to detect and extract. Based on the threshold autoregressive model, pulse linear form, Markov chain Monte Carlo (MCMC), and profile least squares (PrLS) algorithm, phase threshold autoregressive (PTAR) model and double layer threshold autoregressive (DLTAR) model are proposed for detection and extraction of weak pulse signals in chaotic noise, respectively. Firstly, based on noisy chaotic observation, phase space is reconstructed according to Takens's delay embedding theorem, and the phase threshold autoregressive (PTAR) model is presented to detect weak pulse signals, and then the MCMC algorithm is applied to estimate parameters in the PTAR model; lastly, we obtain one-step prediction error, which is used to realize adaptively detection of weak signals with the hypothesis test. Secondly, a linear form for the pulse signal and PTAR model is fused to build a DLTAR model to extract weak pulse signals. The DLTAR model owns two kinds of parameters, which are affected mutually. Here, the PrLS algorithm is applied to estimate parameters of the DLTAR model and ultimately extract weak pulse signals. Finally, accurate rate (Acc), receiver operating characteristic (ROC) curve, and area under ROC curve (AUC) are used as the detector performance index; mean square error (MSE), mean absolute percent error (MAPE), and relative error (Re) are used as the extraction accuracy index. The presented scheme does not need prior knowledge of chaotic noise and weak pulse signals, and simulation results show that the proposed PTAR-DLTAR model is significantly effective for detection and extraction of weak pulse signals under chaotic interference. Specifically, in very low signal-to-interference ratio (SIR), weak pulse signals can be detected and extracted compared with support vector machine (SVM) class and neural network model.

1. Introduction

Weak signals are extremely weak and difficult to detect in most situations. Signal-to-noise ratio (SNR) or signal-to-interference ratio (SIR) is a measure of relative strength of signal and noise [1, 2]. Weak signal detection and extraction firstly need to analyze characteristics of noise and then use modern signal processing methods and statistical models to achieve signal detection and recovery of weak signals inundated by strong noise [3, 4]. The main methods of statistical detection and extraction of weak signals include the stochastic resonance method [5–8], chaotic system and control method [9, 10], neural network method [11], Duffing oscillator method [12–16], and lock phase amplifier method [17]. These traditional methods can be called noise suppression methods and have weak detection capabilities for lower signal-to-noise ratio situations, especially for signal detection that is submerged under chaotic or fractal noise. With the systematic study of characteristics of chaotic or fractal signals, models and methods for characterizing chaos [18, 19] and fractals are continuously updated and iteratively, and these new theories are fully utilized to provide an effective solution to the problem of detection and extraction of weak signals under chaotic noise. The detection and extraction of weak signals under chaotic noise interference can achieve lower SNR working thresholds by fully utilizing chaotic nonlinear characteristics of observation information [20, 21]. It has a wide range of applications in the fields of wireless secure communications, marine monitoring, and bioinformatics [22–28].

Pulse signals are a common signal in the fields of wireless communication, fault diagnosis, ocean monitoring, and bioinformatics [22], which are often interfered by chaotic noise other than Gaussian white noise. How to effectively detect and estimate the weak pulse signal under chaotic noise interference and improve detection limit and extraction accuracy, which are the scientific basis for reducing the cost of testing equipment and the development of high-precision testing instruments, and so it has important theoretical and practical significance. The detection and extraction of weak pulse signals under chaotic interference have become a research hotspot in academic circles, such as neural network methods [29, 30], support vector machine methods [31–33], filter-based methods [34, 35], methods based on empirical mode decomposition [36], geometric methods [37], and local linear methods [38, 39]. These methods have achieved some effects, but often the detection and extraction are separated or the detection does not give an optimal threshold.

In order to realize intelligence statistical detection and improve target signal extraction accuracy of weak pulse signals under chaotic noise, this paper proposes the phase threshold autoregressive (PTAR) model and double layer threshold autoregressive (DLTAR) model for detection and extraction of weak pulse signals in the context of chaotic noise. In signal detection, phase space threshold autoregressive detection (PTAR) model is proposed, which is applied to construct one-step prediction error, hypothesis testing is used to realize detection for weak pulse signals under chaotic noise, and parameters for the PTAR model are obtained by using Markov Chain Monte Carlo (MCMC) method. This method can effectively detect weak pulse signals and increase the adaptive ability. In signal extraction, linear representation of the pulse signal is introduced and mixed into the PTAR model to construct a double layer threshold autoregressive (DLTAR) model, and these parameters are estimated using profile least squares (PrLS) algorithm. The overall framework of this paper is shown in Figure 1:

The structure of this paper is as follows: Section 2 explains weak pulse signal detection based on the PTAR model; Section 3 presents weak pulse signal extraction with the DLTAR model; Section 4 comprises simulation experiment results and analysis; Section 5 concludes the study.

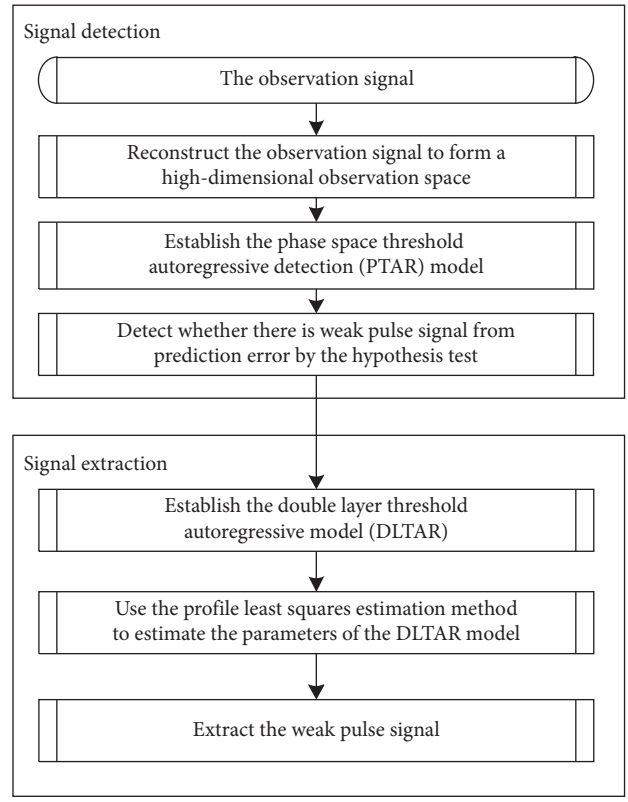

Figure 1: Structure of weak pulse signal detection and extraction in chaotic noise with PTAR and DLTAR models.

2. Weak Pulse Signal Detection Based on the PTAR Model

2.1. Problem Conversion for Signal Detection. Signal detection is a binary decision problem, that is, whether there is a target signal, which is summarized below as a binary hypothesis test:

$$\begin{aligned} H_0 &: r(t) = c(t), \\ H_a &: r(t) = c(t) + s(t), \end{aligned} \tag{1}$$

where $r(t)$ represents the observed signal, $c(t)$ represents chaotic noise, and $s(t)$ represents a weak pulse signal.

Since here the signal-to-noise ratio is extremely low, the target signal is often very weak, and in the case of submerging strong chaotic noise, if the hypothesis test is directly inferred by (1), it is prone to extremely high false positives. Therefore, it is considered to suppress the chaotic noise firstly; that is, if the chaotic noise is known, then (1) can be transformed into the following hypothesis test problem:

$$\begin{aligned} H_0^* &: r(t) - c(t) = 0, \\ H_a^* &: r(t) - c(t) = s(t). \end{aligned} \tag{2}$$

Obviously, chaotic noise is unknown, but its chaotic nonlinear characteristics can be used to obtain its estimation. So one of the key issues in signal detection is how to estimate the chaotic background signal? If the estimation of chaotic noise is obtained, then the residuals can be calculated, and the hypothesis test is used to detect the target signal. The detection model is mainly divided into four steps: (1) reconstructing one-dimensional observation signal to form a high-dimensional observation space and effectively depicting its historical similarity in high-dimensional space; (2) establishing a threshold autoregressive model in phase space for estimating the chaotic noise; (3) calculating the parameters with the MCMC algorithm and obtaining the prediction residuals; (4) using the hypothesis test and p value to detect whether there is a weak pulse signal from prediction error.

2.2. Phase Threshold Autoregressive (PTAR) Model. A one-step prediction model is built in three steps: (1) reconstructing observed signals to form a high-dimensional matrix; (2) forming PTAR model; (3) estimating parameters of the PTAR model by using MCMC algorithm.

2.2.1. Reconstructing Observed Signals to Form High-Dimensional Phase Space. For received signal $\{r(t), t = 1, 2, \ldots, T\}$, its phase in high-dimensional space is

$$R(t) = (r(t), r(t-\tau), \ldots, r(t-(m-1)\tau))', \quad t = t_1, t_1+1, \ldots, T,\ t_1 = 1+(m-1)\tau. \tag{3}$$

According to Takens's theorem [40], there is a smooth mapping $h: R^m \longrightarrow R$ that makes $r(t+1) = h(R(t))$. $(t = t_1, t_1+1, \ldots, T-1)$. If you can find analytical solution of h or find estimate $\widehat{h}$ of h, you can make one-step prediction. Here, the delay time τ is calculated by the complex autocorrelation method, and the embedding dimension m is obtained by the Cao method [41].

2.2.2. Phase Threshold Autoregressive (PTAR) Model. For reconstructed signals $R(t)$, based on a threshold autoregressive model [42], the PTAR model can be expressed as

$$\begin{aligned} r(t+1) &= h_t(R(t)) + \xi(t), \\ h_t(R(t)) &= \sum_{j=1}^{k}\left\{b_0^{(j)} + \sum_{i=1}^{m} b_i^{(j)} r\left(t-(i-1)\tau\right)\right\} I\left(r_{t-d} \in A_j\right) \\ &= \sum_{j=1}^{k}\left[B^{(j)}\right]' \left[\frac{1}{R(t)}\right] I\left(r_{t-d} \in A_j\right), \end{aligned} \tag{4}$$

where $B^{(j)} = (b_0^{(j)}, b_1^{(j)}, \ldots, b_m^{(j)})'$, k is the number of regions, d is the delay parameter, and A_i is divided by the real axis, $A_i = (\gamma_{i-1}, \gamma_i]$, and the variance of $\xi(t)$ is σ^2. The parameters in the model are recorded as $\vartheta = (B^{(j)}, k, d, \gamma_j, \sigma^2)'$.

2.2.3. Parameters Estimation for the PTAR Model. The parameters estimation of the PTAR model is based on the MCMC algorithm. Let $k = 2, \gamma_0 = -\infty, \gamma_1 = \gamma, \gamma_2 = +\infty$, and $d_0 = (m-1)\tau$. The key to the MCMC algorithm is to obtain the posterior distribution of each parameter in $\vartheta = (B^{(j)}, k, d, \gamma_j, \sigma^2)' = (B^{(j)}, d, \gamma, \sigma^2)'$, $j = 1, 2$. The prior distributions of the parameters in the PTAR model are $B^{(j)} \sim i.i.d.N(B_{0j}, V_j^{-1})$; $d \sim U(\{1\}, \{2\}, \ldots, \{d_0\})$ is the discrete uniform distribution; $\gamma \sim U(a, b)$; $\sigma^2 \sim \mathrm{IG}(\alpha, \beta)$ is the inverse gamma distribution; and $(a, b, \alpha, \beta)'$ is a hyperparameter.

According to Chen's literature method [42], conditional posterior distribution of each parameter in the PTAR model is calculated:

$$\left(B^{(j)} \,\middle|\, d, \gamma, \sigma^2\right) \sim i.i.d.N\left(B_j^*, V_j^{*-1}\right), \tag{5}$$

where $B_j^* = (((X_j^{*'} X_j^*)/\sigma^2) + V_j)(((X_j^{*'} X_j^*)/\sigma^2)\widehat{B}_j + V_j B_{0j})$, $X_1^* = (x_{1,\pi_1+d}, x_{1,\pi_2+d}, \ldots, x_{1,\pi_s+d})'$, $X_2^* = (x_{2,\pi_{s+1}+d}, x_{2,\pi_{s+2}+d}, \ldots, x_{2,\pi_{n-d_0}+d})'$, $x_{i,t} = (1, r(t), \ldots, r(t-d_0))'$, $\widehat{B}_j = (X_j^{*'} X_j^*)^{-1} X_j^{*'} R_j^*$, s satisfies $r_{\pi_s} \le \gamma < r_{\pi_s+1}$, $R_1^* = (r_{\pi_1+d}, r_{\pi_2+d}, \ldots, r_{\pi_s+d})'$, and $R_2^* = (r_{\pi_{s+1}+d}, r_{\pi_{s+2}+d}, \ldots, r_{\pi_T-d_0+d})'$.

$$\left(d \mid B^{(j)}, \gamma, \sigma^2\right) \sim \frac{L(r \mid \vartheta)}{\sum_{d=1}^{d_0} L\left(r \mid B^j(t), d, \gamma, \sigma\right)^2}, \tag{6}$$

where $L(r \mid \vartheta) = L(r \mid B^{(j)}, d, \gamma, \sigma^2) = \exp(-s_r^2/2\sigma^2)/\sigma^{T-d_0}$ and $s_r^2 = \sum_{j=1}^{2}(R_j^* - X_j^{*'} B^{(j)})'(R_j^* - X_j^{*'} B^{(j)})$.

$$\left(\gamma \mid B^{(j)}, d, \sigma^2\right) \sim \exp\left\{-\frac{s_r^2}{2\sigma^2}\right\}, \quad I(a < \gamma < b), \tag{7}$$

$$\left(\sigma^2 \,\middle|\, B^{(j)}, d, \gamma\right) \sim \mathrm{IG}\left(\alpha + \frac{T-d_0}{2}, \beta + \frac{s_r^2}{2}\right). \tag{8}$$

According to the above posterior distribution, Gibbs sampling and random walk M-H sampling algorithm [42] are used to estimate the mean of parameters. The specific sampling plan is as follows:

(1) Sampling by using the Gibbs sampling method based on the posterior distribution (5)

(2) Sampling by using the Gibbs sampling method based on the posterior distribution (6)

(3) Sampling by using the random walk M-H sampling method based on the posterior distribution (7)

(4) Sampling by using the Gibbs sampling method based on the posterior distribution (8)

Using this sampling scheme, iteratively calculate 10,000 times, burn the first 4000 times, and use subsequent stable Markov chain to calculate the sample mean of each parameter; that is, the parameter estimation is obtained.

Bring the estimated value $\widehat{\vartheta}$ of ϑ into the PTAR model to obtain one-step predicted value $\widehat{r}(t+1) = h_t(R(t), \widehat{\vartheta})$, and then prediction error $e(t+1)$ is

$$e(t+1) = r(t+1) - \widehat{r}(t+1) = r(t+1) - h_t(R(t), \widehat{\vartheta}). \tag{9}$$

2.3. PTAR Statistical Detection Method for Weak Pulse Signals. Based on the prediction error obtained in Section 2.2, a hypothesis test is performed to determine whether there is a weak pulse signal $s(t)$ in observed signal $r(t)$. Based on prediction error equation (9), we get statistics $D_0 = (e(t) - \overline{e}(t))/s_{e(t)}$ and $D_0 \sim t(T-1-d_0)$ (under the condition that H_0 is established), and then the p value at time t is $p_t = P_{H_0}(|D| > |D_0(t)|)$, where $D_0(t)$ is the sample implementation value of D_0 under assumption that the null hypothesis is established. At a significance level of 0.05, the optimal detection threshold is $t_{0.025}(T-1-d_0)$. The weak signal is detected by the p value. If $p < 0.05$, the null hypothesis is rejected, and there is a weak pulse signal; otherwise, it does not exist.

The weak pulse detection process based on the PTAR model and hypothesis test method is shown in Figure 2.

3. Weak Pulse Signal Extraction with the DLTAR Model

3.1. Double Layer Threshold Autoregressive (DLTAR) Model. The weak pulse signal here is a multipoint skip pulse model formed by plurality of pulses at different time points, as follows:

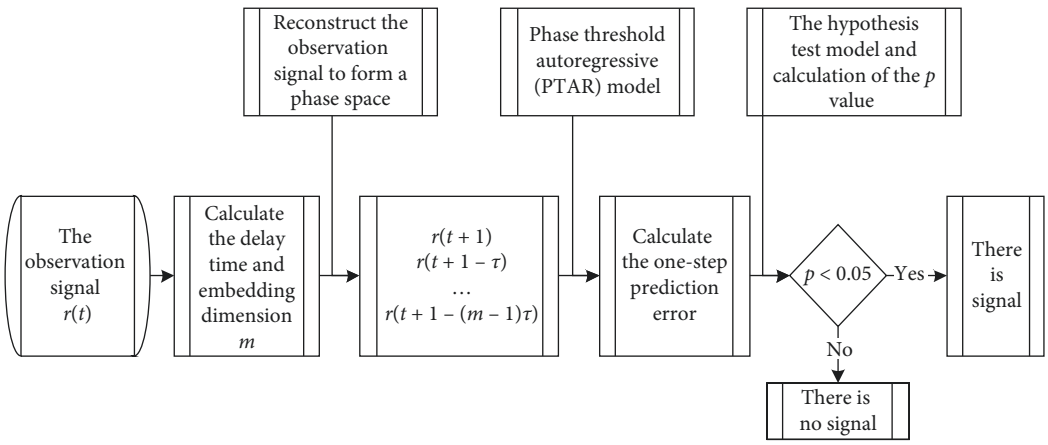

Figure 2: Flowchart of the PTAR detection model.

$$s(t) = \sum_{i=1}^{p} a_i s_i(t) = A'\tilde{s}(t), \tag{10}$$

where $s_i(t) = \begin{cases} 1, & t = T_i \\ 0, & \text{else} \end{cases}$, $\tilde{s}(t) = (s_1(t), s_2(t), \ldots, s_p(t))'$, and $A = (a_1, a_2, \ldots, a_p)'$.

According to basic principle described in Section 2, combined with linear representation of the weak pulse signal and PTAR model, the following extraction model is established:

$$\begin{cases} \tilde{c}(t) = r(t) - A'\tilde{s}(t), \\ \tilde{c}(t+1) = h_t(\tilde{C}(t)) + \varepsilon(t). \end{cases} \tag{11}$$

The above model is called the double layer threshold autoregressive (DLTAR) model. This model is novel, and it combines the hot spot and PTAR model of the pulse signal and contains the parametric and nonparametric parts. So it cannot be solved directly. Among them, $\tilde{C}(t) = (\tilde{c}(t), \tilde{c}(t-\tau), \ldots, \tilde{c}(t-(m-1)\tau))'$ and $\varepsilon(t)$ is the Gaussian white noise with zero mean. It can be seen from formula (11) that the DLTAR model contains parameter vector A and the nonparametric part h_t. From linear expression of the weak pulse signal, it is known that if A is obtained, then signal $s(t)$ is extracted. The parameters in the DLTAR model are estimated by using the profile least squares estimation (PrLS) method.

3.2. Estimating Parameters of the DLTAR Model with the PrLS Method. If least square estimation method is used and sum of squared errors of the DLTAR model is minimized, then the optimal estimate can be obtained, namely,

$$\begin{aligned} \hat{A} &= \arg\min_{A} \sum_{t=n_1}^{T-1} \left[\tilde{c}(t+1) - h_t(\tilde{C}(t))\right]^2 \\ &= \arg\min_{A} \sum_{t=n_1}^{T-1} [r(t+1) - A'\tilde{s}(t+1) \\ &\quad - h_t(r(t) - A'\tilde{s}(t), \ldots, r(t-(m-1)\tau) - A'\tilde{s}(t-(m-1)\tau)]. \end{aligned} \tag{12}$$

It is known from (12) that it contains two major unknown parameters A and h_t, and the form of h_t is more complicated. Here, the profile least squares (PrLS) algorithm [43] is used to alternately update iterative estimates of A and h_t.

The procedure for estimating optimal values of parameters A and h_t by using the PrLS algorithm is divided into three steps: (1) calculating h_t with the values of A with the MCMC algorithm; (2) the value of A iteratively is updated with the value of h_t with the PrLS algorithm; and (3) the alternate iteration is repeated until the value of A changes very little or the specified error is reached. The detailed steps are described as follows:

(a) Given the initial value $A^{(n)}$ $(n = 1, 2, 3, \ldots)$ of A, estimate the value of h_t, denoted as $h_t^{(n)}$.

It can be seen from equation (11) that when a value of A is given, $\tilde{c}(t)$ can be calculated. The structure is the analogy of the PTAR detection model. Take the MCMC algorithm to estimate, as follows:

$$h_t^{(n)} = \left\{\tilde{c}(t+1) = r(t+1) - \left(A^{(n)}\right)'\tilde{s}(t) = h_t(\tilde{C}(t)) + \varepsilon(t)\right\}$$

model's MCMC estimation. (13)

(b) Update the value of A with value $h_t^{(n)}$ of h_t estimated in (a) and record it as $A^{(n+1)}$.

It can be seen from equation (12) that when h_t is given, the optimal value of A can be obtained by using the Newton–Raphson algorithm. The specific description is as follows:

$$\begin{aligned} L(A) &= \sum_{t=t_1}^{T-1} \left[\tilde{c}(t+1) - h_t(\tilde{C}(t))\right]^2 \\ &= \sum_{t=t_1}^{T-1} \left[r(t+1) - A's(t+1) - h_t(\tilde{C}(t))\right]^2. \end{aligned} \tag{14}$$

Let $\dot{L}(A) = 0$, where $\dot{L}(\cdot)$ is the derivative. For a given $A^{(n)}$, according to Taylor's exhibition, there is

$$0 = \dot{L}(A) \approx \dot{L}\left(A^{(n)}\right) + \ddot{L}\left(A^{(n)}\right)\left(A - A^{(n)}\right). \tag{15}$$

From (15), there is one-step iteration formula:

$$A^{(n+1)} = A^{(n)} - \left[\ddot{L}\left(A^{(n)}\right)\right]^{-1}\dot{L}\left(A^{(n)}\right). \tag{16}$$

(c) Repeating steps (a) and (b) until $A^{(n)}$ converges to obtain optimal estimate A.

3.3. Implementation of Weak Pulse Signal Extraction for the DLTAR Model. According to the foregoing, the DLTAR model is implemented in the form of pseudocode and process structure diagram for weak pulse signal extraction. The pseudocode (Algorithm 1) is as follows, and the extracted process structure is shown in Figure 3.

4. Simulation Experiment Results and Analysis

Experimental environment is as follows: Intel CPU Core i3 processor, main frequency 3.2 GHz, memory 4 GB, 32-bit Windows 7 operating system, R 3.5.1 programming environment.

In simulation experiment, Lorenz and Rossler system is used to generate chaotic noise, and the signal-to-interference ratio (SIR) is used to measure signal and interference strength. Accuracy rate (Acc), ROC curve (receiver operating characteristic curve), and AUC (area under ROC curve) are used to evaluate performance evaluation criteria of detector. Relative error (Re), mean square error (MSE), and mean absolute percentage error (MAPE) are used as extraction accuracy.

(1) SIR $= 10\log(\sigma_s^2/(\sigma_c^2 + \sigma_w^2))$

(2) ACC $= (\mathrm{TP} + \mathrm{TN})/(\mathrm{TP} + \mathrm{TN} + \mathrm{FP} + \mathrm{FN})$

(3) ROC: dichotomous problem evaluation index, with FPR as the abscissa and TPR as the ordinate

(4) AUC: area under ROC curve

(5) MSE $= (1/T)\sum_{t=1}^{T}(s(t) - \hat{s}(t))^2$

(6) MAPE $= (1/T)\sum_{t=1}^{T}|(s(t) - \hat{s}(t))/\hat{s}(t)|$

(7) Re $= |(s(t) - \hat{s}(t))/\hat{s}(t)|$

where $\sigma_s^2 = 1/T\sum_{t=1}^{T}(s(t) - \overline{s}(t))^2$, $\sigma_c^2 = 1/T\sum_{t=1}^{T}(c(t) - \overline{c}(t))^2$, $\overline{s}(t)$ and $\overline{c}(t)$ are the mean values of $s(t)$ and $c(t)$, σ_w^2 is the variance of the white noise $w(t)$, TP is the number of times that there is a pulse signal and is judged to have a pulse signal, TN is the number of times that there is no pulse signal and is judged to be no pulse signal, FP is the number of times that there is a pulse signal when there is no pulse signal, and FN is the number of times when there is a pulse signal to determine that there is no pulse signal, TPR = TP/(TP + FN), and FPR = FP/(FP + TN).

Lorenz system equation is as follows:

$$\begin{cases} \dot{c} = \sigma(y - c), \\ \dot{y} = -cz + rc - y, \\ \dot{z} = cy - bz, \end{cases} \tag{17}$$

where c, y, z is a function of time and parameters, $\sigma = 10$, $b = 8/3, r = 28, c(0) = 1, y(0) = 1, z(0) = 1$, and sampling time is $t = 0.01$ second, which is solved by the fourth-order Runge–Kutta method. Take 3000 to 7000 points to represent chaotic noise, denoted by $\{c(t), t = 1, 2, \ldots, 4000\}$.

Rossler system equation is as follows:

$$\begin{cases} \dot{c} = -y - z, \\ \dot{y} = c + a_1 * y, \\ \dot{z} = b_1 + z*(c - c_1), \end{cases} \tag{18}$$

where c, y, z is a function of time and parameters $a_1 = 0.2, b_1 = 0.2$, and $c_1 = 8/3, c(0) = 1, y(0) = 1, z(0) = 1$, and sampling time is $t = 0.01$ second, which is solved by the fourth-order Runge–Kutta method. Take 3000 to 7000 points to represent chaotic noise, denoted by $\{c(t), t = 1, 2, \ldots, 4000\}$.

The delay time and embedding dimension of observed signals are calculated according to the complex autocorrelation method and Cao method [41] ($\tau = 7, m = 6$).

4.1. Experiment 1: Detection Experiment for the PTAR Model. Take transient pulse signals at eight different times, $s(t) = \sum_{i=1}^{8} a_i s_i(t)$, where $a_i = 6.5$,

$$s_i(t) = \begin{cases} 1, & t = T_i,\ T_i \in \{450, 900, 1350, 1800, 2250, 2700, \\ & 3150, 3600\}, \\ 0, & \text{otherwise}, \end{cases} \tag{19}$$

and pulse signal data of length 4000 is generated by formula (19); at this time, SIR reaches −65.9707 dB.

(1) The pulse signal is detected by the PTAR model, and the detection result is shown in Figures 4 and 5.

Figures 4 and 5(a) show the original chaotic noise signal, Figures 4 and 5(b) show the superimposed chaotic noise and the observed signal of target signal, Figures 4 and 5(c) show the one-step fitting prediction error of the PTAR model, and Figures 4 and 5(d) show a plot of the p value of test statistic D. Comparing Figures 4 and 5(a) with Figures 4 and 5(b), the observed signal is basically consistent with nonlinear chaotic characteristics of chaotic noise; that is to say, weak pulse signals do not fundamentally change the structure of chaotic attractor; therefore, the signal reconstruction is basically not affected, and the historical similarity of phase points in chaotic high-dimensional space can be effectively utilized to perform model fitting. From the residual value in Figures 4 and 5(c), the moment with pulse signals has a large error, which can be judged by the naked eye. However, in order to adapt to adaptive judgment of machine, the p value is further calculated here, as shown in Figures 4 and 5. It can be seen from the p value in Figures 4 and 5(d) that the p value is lower than the critical value at the time of pulse signals, and the weak pulse signals at different times can be effectively detected. At this one time detection, Acc is 100%. So the PTAR model is effective for different chaotic noise backgrounds.

(2) Comparison results of ROC curves under different models are shown in Figure 6. Here, we compare the LS-SVM model (abbreviated as LS-SVM) [26] and RBF

Inputs: observed signal data with chaotic noise and parameters k, τ, m, etc.
Outputs: the optimal value of the parameters A and h_t and the weak pulse signal $s(t)$.
Begin
Standardize raw data and reconstruct phase space
Initialization of parameters such as A and d_0.
Initialize the distribution, such as $B^{(j)} \sim i.i.d.N(B_{0j}, V_j^{-1})$; $d \sim U(\{1\}, \{2\}, \ldots, \{d_0\})$ is discrete uniform distribution; $\gamma \sim U(a, b)$; $\sigma^2 \sim \mathrm{IG}(\alpha, \beta)$ is the inverse gamma distribution.
While $(|A^{(n+1)} - A^{(n)}| > 10e - 3)$
  Check for the presence of $s(t)$ according to Section 2;
  Calculate $h_t^{(n)}$ according to the DLTAR model constructed according to (13);
  Updating the parameter $A^{(n)}$ with the profile least squares algorithm;
  Bring the estimated $A^{(n)}$ into the pulse signal and calculate $s(t)$;
$n + 1 \longleftarrow n$
End while
Output the optimal parameter value, and calculate the weak pulse signal.
End
Note: (1) The delay time and embedding dimension remain unchanged. Since $s(t)$ is a weak signal, the delay time and embedding dimension in phase space reconstruction are basically not affected. (2) When calculating the derivative, a differential algorithm is used because all data is discretized.

Algorithm 1

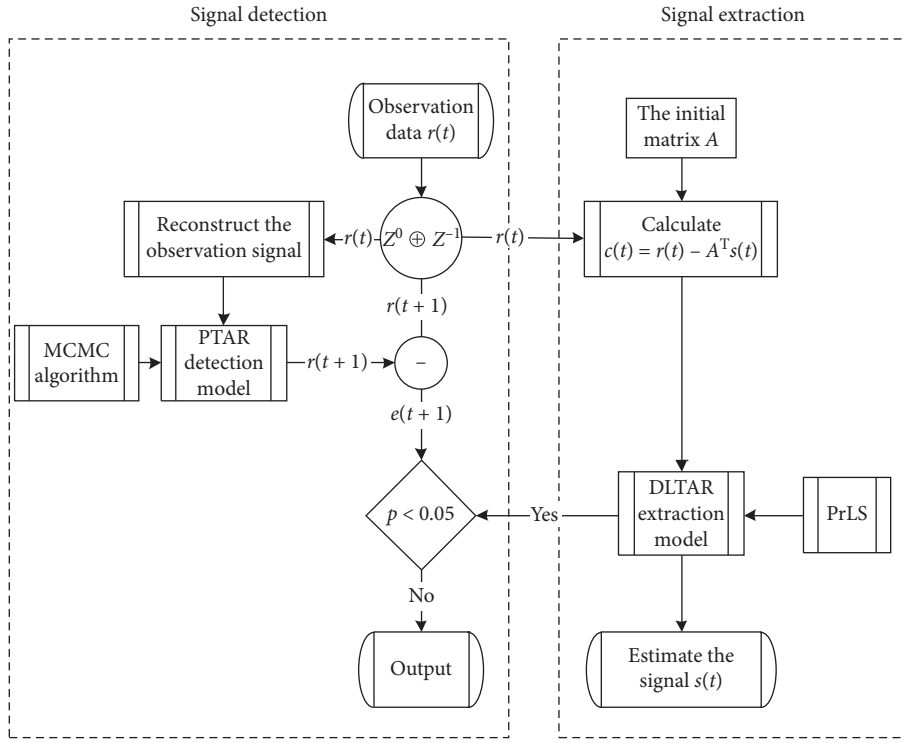

Figure 3: Realization of weak pulse signal extraction with the DLTAR model.

neural network model (abbreviated as RBF-NN) [29]. It can be seen from Figure 6 that the PTAR detection model is optimal. AUC values of three detection methods are 0.9987 (PTAR), 0.9862 (LS-SVM), and 0.9571 (RBF-NN), which further quantify that performance of the detection model in this paper is superior.

4.2. Experiment 2: Extraction Experiment of Weak Pulse Signals. It is assumed that 4000 points of observation signal $r(t)$ contain pulse signals of different amplitudes at 10 times, and the extraction results of the DLTAR model are shown in Figure 6 and Table 1.

Table 1 shows the extracted results of DLTAR models for 10 different moments and different amplitudes. From relative error (Re), the magnitude scale is $10e - 5$, the maximum relative error is 0.014%, and the minimum relative error is $0.31746e - 5$. Therefore, the extraction accuracy based on the DLTAR model is high, the relative error is

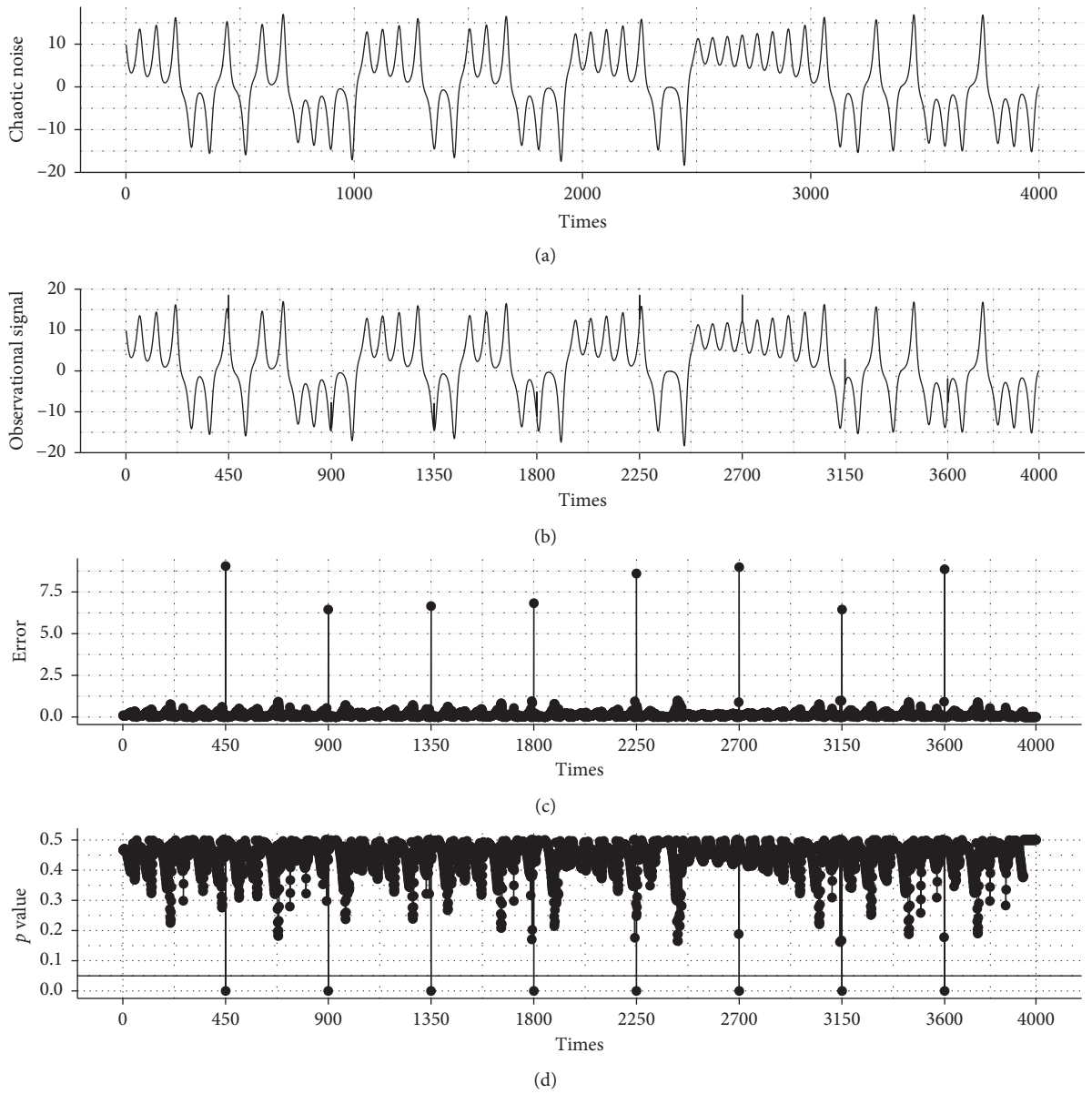

Figure 4: Detection results based on the PTAR model for the Lorenz system: (a) original chaotic noise $c(t)$; (b) observational signal $r(t)$; (c) fitting prediction error $e(t)$; (d) p value.

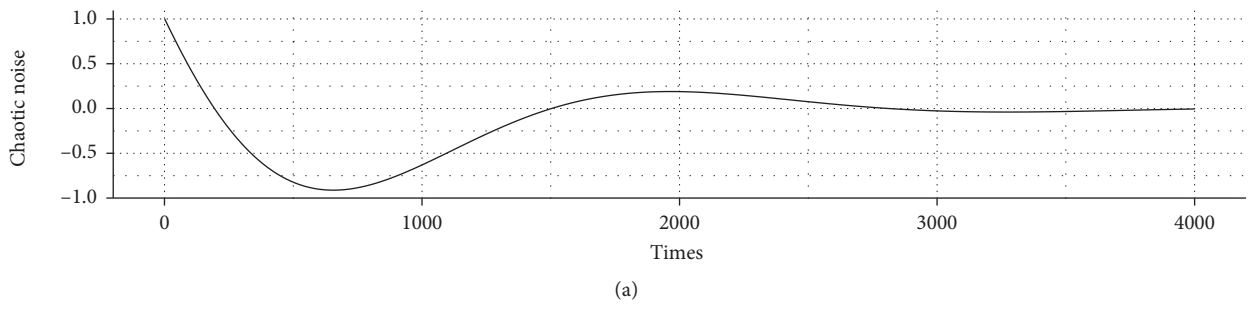

Figure 5: Continued.

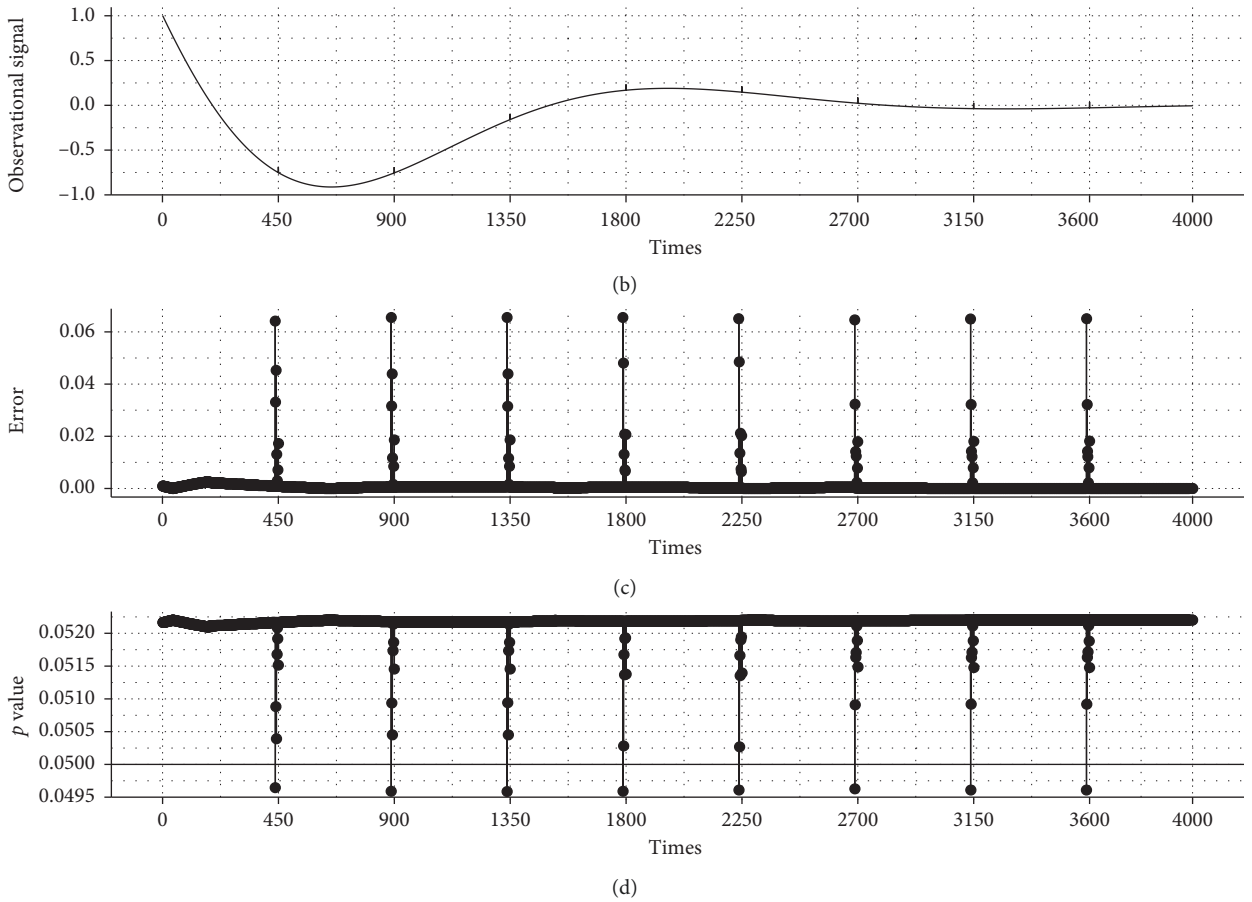

Figure 5: Detection results based on the PTAR model for the Rossler system: (a) original chaotic noise $c(t)$; (b) observational signal $r(t)$; (c) fitting prediction error $e(t)$; (d) p value.

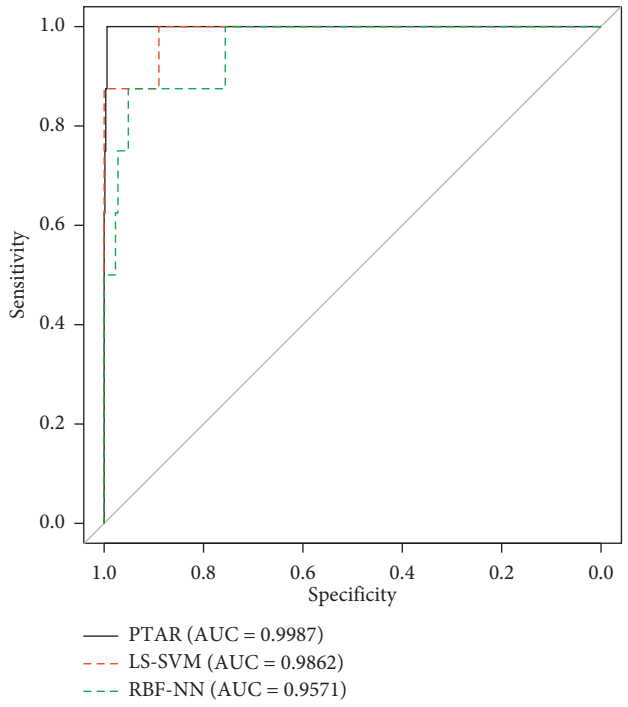

Figure 6: ROC curve with three different models.

Table 1: Results of weak signal extraction with the DLTAR model.

t	True value	Extracted value	Relative error
700	5.2000	5.20009	$1.73077e-5$
1300	5.5000	5.50008	$1.45455e-5$
1600	6.5000	6.50008	$1.23077e-5$
1900	6.0000	6.00026	$4.33333e-5$
2100	6.5000	6.50091	0.0001400
2500	7.0000	7.00034	$4.85714e-5$
3000	6.4000	6.39989	$1.71875e-5$
3400	6.3000	6.29998	$0.31746e-5$
3700	6.2000	6.19990	$1.61290e-5$
3900	7.5000	7.49990	$1.33333e-5$

within the acceptable range, and the extracted performance is excellent. Specific estimation results, mean square error (MSE), and mean absolute percentage error (MAPE) are as shown in Figure 6.

Since the extracted value is close to the true value, the extracted value in Figure 7(a) is offset to the right by 30 display units, and SIR is −64.2382 dB. Figures 7(b) and 7(c) show the iterative convergence curves of MSE and MAPE. MSE approximately converges to $0.1065e-05$, and MAPE approximately converges to $0.032587e-03$ and converges around 40 steps.

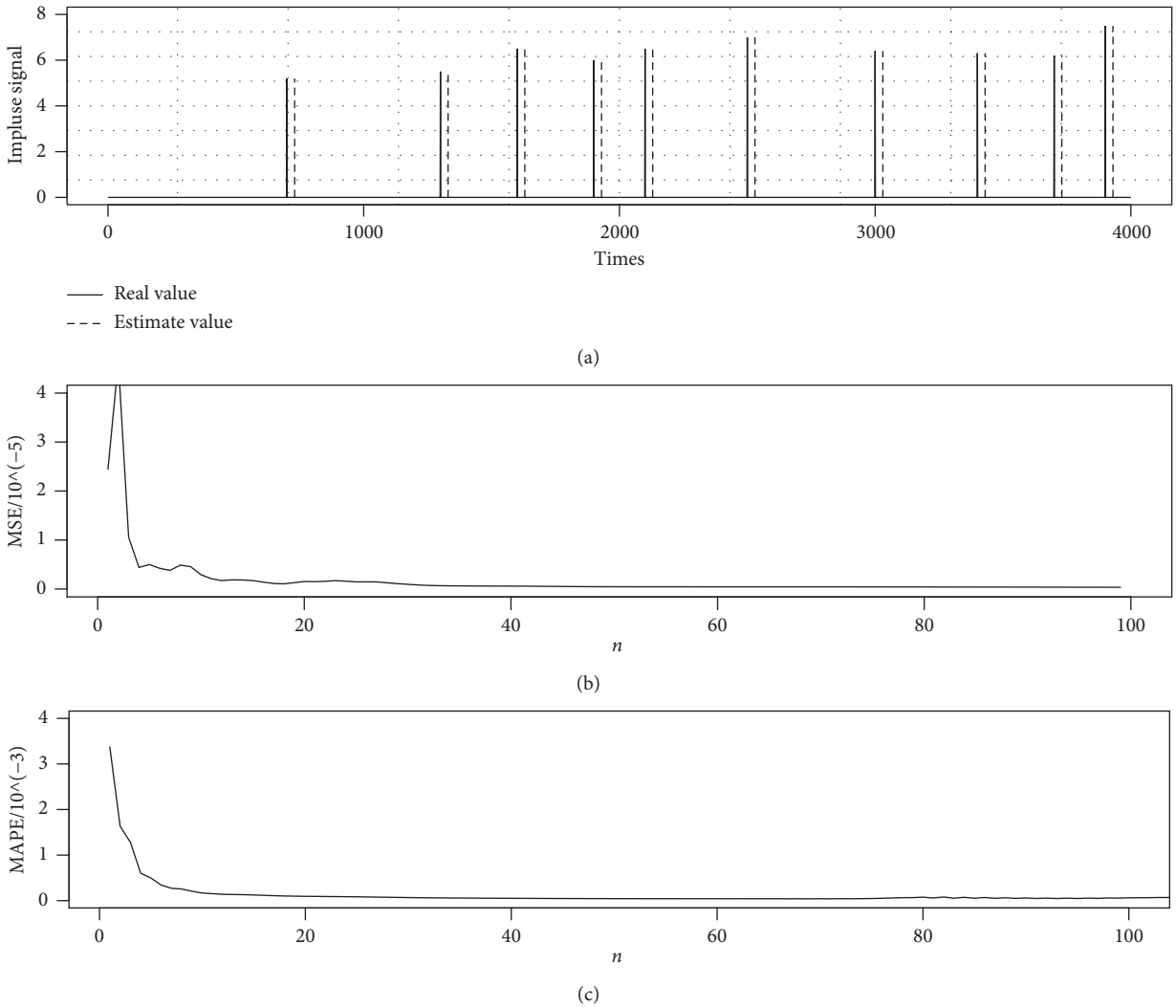

Figure 7: Extraction results of different times and different amplitudes with the DLTAR model: (a) comparison of the real value and extracted value; (b) MSE curve of the pulse signal; (c) MAPE curve of the pulse signal.

4.3. Experiment 3: Pulse Signal Extraction Experiment Based on the PTAR-DLTAR Model with Different SIRs. Considering weak pulse signals in the case of ten different pulse magnitudes, the pulse signals in each case are composed of four pulse signals at different time points, and the signal-to-interference ratio (SIR) is adjusted by changing the magnitude of pulse intensity. 4000 points of the observed signal is selected as sample, and the experimental results are shown in Table 2:

From Table 2, the pulse signal amplitude is from strong to weak. At this time, SIR is high to low, and extraction accuracy of the DLTAR model is degraded. When SIR is greater than −124 dB, MSE and MAPE are relatively small, and extraction of the weak pulse signal is better. However, when SIR is less than −124 dB, the accuracy of MSE and MAPE is significantly reduced. At this time, the DLTAR model gradually loses its effect probably because the pulse signal is too weak relative to the noise so that the target signal value cannot be effectively extracted and is suppressed as noise. Therefore, when SIR is higher than −124 dB, the DLTAR model is superior in recovering the weak pulse signal. At this time, both MSE and MAPE are relatively small, so DLTAR estimation model can realize the recovery of weak pulse signals under extremely low signal-to-interference ratio.

4.4. Experiment 4: Performance Comparison with SVM-Based and Neural Network-Based Estimation Models. This paper compares common machine learning estimation methods, such as dual-constrained LS-SVM model (abbreviated as D-SVM), GA-SVM model (abbreviated as GA-SVM), and LS-SVM model (abbreviated as LS-SVM) [26], and the RBF neural network model (abbreviated as RBF-NN) [29]. The pulse signal takes a value of

$$s(t) = \begin{cases} 1.5, & t = 3001, 3002, \ldots, 3010, \\ 0, & \text{otherwise}, \end{cases} \tag{20}$$

using the signal-to-interference ratio and mean square error for comparative analysis of extracted performance. The specific results are shown in Figure 8 and Table 3.

Table 2: Results of pulse signal extraction with different SIRs.

a_i, (i = 450, 900, 1350, 1800)	SIR (dB)	MSE	MAPE
75.0	−23.97844	1.315e − 06	7.049e − 05
35.0	−39.22124	1.492e − 06	8.786e − 05
25.0	−45.95068	1.537e − 06	8.255e − 05
15.0	−56.16719	1.714e − 06	8.349e − 05
10.0	−64.27650	1.865e − 06	8.202e − 05
5.50	−76.23324	1.912e − 06	12.72e − 05
2.50	−92.00238	2.028e − 05	9.308e − 04
1.50	−102.2189	2.155e − 04	9.679e − 03
0.50	−124.1911	2.661e − 04	21.07e − 03
0.05	−170.2428	3.069e − 03	24.93e − 02

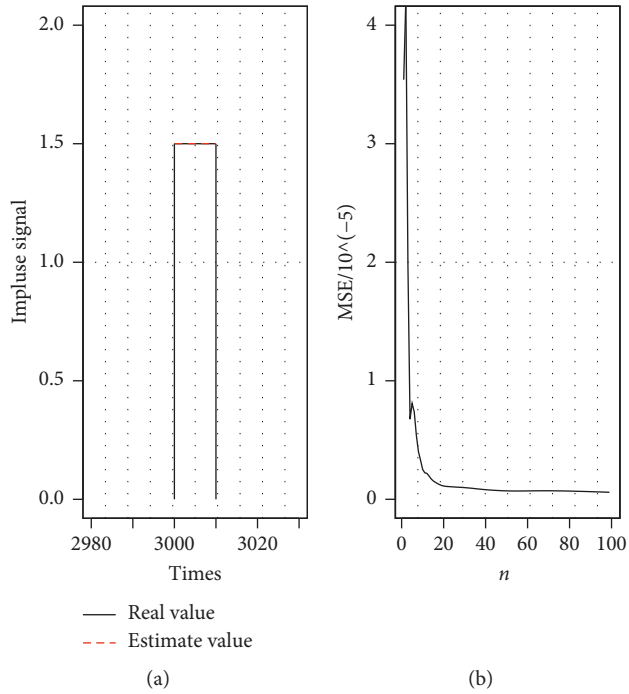

Figure 8: . Extraction results of weak pulse signal with DLTAR: (a) comparison of real value and extracted value; (b) MSE curve of the pulse signal.

Table 3: Performance comparison of SVM-class and RBF neural network models.

	PTAR	D	GA	LS	RBF
SIR (dB)	−92.12	−77.33	−89.7704	−62.82	−30.20
MSE	1.058e − 06	6.400e − 05	2.45e − 05	0.0484	0.0336

It can be seen from Figure 8 and Table 3 that when SIR reaches −92.12 dB, the estimated performance is excellent, the estimated value and the true value are in controllable range, the true value is 1.5, the estimated value is 1.50023, and MSE is 0.1058e − 05. Compared with support vector machine and RBF neural network model, the estimation accuracy for the presented method is higher and signal-to-interference ratio is lower. The specific results are shown in Table 3.

5. Conclusions

Aiming at the detection and extraction of weak pulse signals under strong chaotic noise, nonlinear characteristics of chaos and linear representation of pulse signals are combined to construct the phase space threshold autoregressive detection model (PTAR detection model) and double layer threshold autoregressive extraction model (DLTAR extraction model). The extraction model built in this paper is directly related to the detection model, adopts the same model structure, and does not require additional prior knowledge. It can realize the detection and extraction of weak pulse signals under extremely low signal-to-interference ratio, which is efficient and easy. It can be known from the simulation experiment results that the PTAR detection model can effectively detect weak pulse signals from

chaotic noise. The DLTAR extraction model has excellent extraction performance and high precision. Its relative error is less than 0.014%, mean square error is not higher than $0.1065 * 10e - 5$, and MAPE is as low as $0.32587 * 10e - 4$. It can be seen from the detection and extraction experiments of pulse signals under different signal-to-interference ratios that the PTAR-DLTAR model can achieve a lower signal-to-interference ratio working threshold in the background of chaotic noise and mean square error of extraction accuracy is maintained at the $10e - 4$ magnitude level; that is, when SIR is −124.19 dB, MSE is $2.661 * 10e - 4$. Compared with support vector machine and RBF neural network model, the detection ability of the proposed model is stronger and the extraction effect is better.

Data Availability

The data used to support the findings of this study are available from the corresponding author upon request.

Conflicts of Interest

The authors declare that there are no conflicts of interest regarding the publication of this paper.

Acknowledgments

This paper was supported by the Fundamental and Advanced Research Project of CQ CSTC of China (Grant no. cstc2018jcyjX0464), National Natural Science Foundation of China (Grant nos. 11871124 and 11471060), and Chongqing University of Technology Foundation (Grant no. 2016ZD33).

References

[1] G. Wang, D. Chen, J. Lin, and X. Chen, "The application of chaotic oscillators to weak signal detection," *IEEE Transactions on Industrial Electronics*, vol. 46, no. 2, pp. 440–444, 1999.

[2] C. Nie and Y. Shi, "The research of weak signal detection based on cross-correlation and chaos theory," *Chinese Journal of Scientific Instrument*, vol. 22, no. 1, pp. 32–35, 2001.

[3] K. M. Hock, "Narrowband weak signal detection by higher order spectrum," *IEEE Transactions on Signal Processing*, vol. 44, no. 4, pp. 874–879, 1996.

[4] G. Wang, H. Zhang, F. Zhang, and J. Ye, "Scale transformation for detecting transient electromagnetic weak signal of stochastic resonance," *Chinese Journal of Geophysics*, vol. 54, no. 7, pp. 1928–1934, 2011.

[5] Q. He and J. Wang, "Effects of multiscale noise tuning on stochastic resonance for weak signal detection," *Digital Signal Processing*, vol. 22, no. 4, pp. 614–621, 2012.

[6] S.-L Gao, S.-C Zhong, W. Wei, and H. Ma, "Weak signal detection based on chaos and stochastic resonance," *Acta Physica Sinica*, vol. 61, no. 18, Article ID 180501, 2012.

[7] D. Han, X. Ding, and P. Shi, "Multi-frequency weak signal detection based on EMD after de-noising by adaptive re-scaling frequency-shifted band-pass stochastic resonance," *Journal of Mechanical Engineering*, vol. 49, no. 8, pp. 10–18, 2013.

[8] J. Fan, W.-L Zhao, M.-L Zhang, R.-H Tan, and W.-Q Wang, "Nonlinear dynamics of stochastic resonance and its application in the method of weak signal detection," *Acta Physica Sinica*, vol. 63, no. 11, Article ID 110506, 2014.

[9] L. Pei, J. Kuang, and S. Yuan, "Frequency characteristics and weak signal detection of chaotic synchronization systems," *Science in China Series E: Technological Sciences*, vol. 40, no. 3, pp. 237–242, 1997.

[10] L. Yue and B. Yang, "Chaotic system for detecting periodic signals in the background of strong noise," *Chinese Science Bulletin*, vol. 48, no. 5, pp. 508–510, 2003.

[11] J. He, Z. Yang, and S. Wang, "Transient signal detetion based on chaos and neural network," *Acta Electronica Sinica*, vol. 26, no. 10, pp. 33–37, 1998.

[12] T. Jin and H. Zhang, "Statistical approach to weak signal detection and estimation using Duffing chaotic oscillators," *Science China Information Sciences*, vol. 54, no. 11, pp. 2324–2337, 2011.

[13] X. Deng, H. Liu, and T. Long, "A new complex Duffing oscillator used in complex signal detection," *Chinese Science Bulletin*, vol. 57, no. 17, pp. 2185–2191, 2012.

[14] G. Yan, Y. Zhang, J. Miao, W. Zhang, and T. Shi, "A weak signal detection method by duffing system with the gain," *Acta Electronica Sinica*, vol. 40, no. 6, pp. 1269–1273, 2012.

[15] X. Zhou, L. Lai, and Y. Luo, "A new detecting method for periodic weak signals based on fractional order stopping oscillation system," *Acta Physica Sinica*, vol. 62, no. 9, Article ID 090501, 2013.

[16] L. Meng-Ping, X. Xue-Mei, Y. Bing-Chu, and D. Jia-Feng, "A circular zone counting method of identifying a Duffing oscillator state transition and determining the critical value in weak signal detection," *Chinese Physics B*, vol. 24, no. 6, Article ID 060504, 2015.

[17] Y. Nie, X. Xu, B. Li, and B. Yang, "Weak signal detection method based on lock-in amplifier," *Chinese Journal of Sensors and Actuators*, vol. 26, no. 9, pp. 1243–1247, 2013.

[18] L.-Y. Su, "Prediction of multivariate chaotic time series with local polynomial fitting," *Computers & Mathematics with Applications*, vol. 59, no. 2, pp. 737–744, 2010.

[19] Li-Y. Su, M. Yan-Ju, and L. Jiao-Jun, "Application of local polynomial estimation in suppressing strong chaotic noise," *Chinese Physics B*, vol. 21, no. 2, Article ID 020508, 2012.

[20] L. Su and C. Li, "Extracting narrow-band signal from a chaotic background with LLVCR," *Wireless Personal Communications*, vol. 96, no. 2, pp. 1907–1927, 2017.

[21] L.-Y. Su, H.-H. Sun, J. Wang, and L.-M. Yang, "Detection and estimation of weak pulse signal in chaotic background noise," *Acta Physica Sinica*, vol. 66, no. 9, Article ID 090503, 2017.

[22] L. Yue, B. Yang, Y. Yuan, X. Zhao, and H. Lin, "Weak effective seismic signal detection capability of chaotic oscillator detection system," *Chinese Science Bulletin*, vol. 51, no. 14, pp. 1710–1716, 2006.

[23] P. Du, Y. Wang, and W. Sun, "Weak signal detection in the background of chaotic sea clutter," *Systems Engineering and Electronics*, vol. 7, pp. 65–67, 2001.

[24] H.-Y. Xing and T.-L. Jin, "Weak signal estimation in chaotic clutter using wavelet analysis and symmetric LS-SVM regression," *Acta Physica Sinica*, vol. 59, no. 1, pp. 140–146, 2010.

[25] J.-B. He, Z. Liu, and S.-L. Hu, "Detection of weak signal based on the sea clutter scattering," *Acta Physica Sinica*, vol. 60, no. 11, Article ID 110208, 2011.

[26] H.-Y. Xing, Q.-Q. Zhu, and W. Xu, "A method of weak target detection based on the sea clutter," *Acta Physica Sinica*, vol. 63, no. 10, Article ID 100505, 2014.
[27] H.-Y. Xing, Q. Zhang, and W. Xu, "Hybrid algorithm for weak signal detection in chaotic sea clutter," *Acta Physica Sinica*, vol. 64, no. 4, Article ID 040506, 2015.
[28] Q.-Q. Li, X.-M. Xu, L.-Z. Yin, Y.-P. Ding, J.-F. Ding, and K.-H. Sun, "Implication of two-coupled tri-stable stochastic resonance in weak signal detection," *Chinese Physics B*, vol. 27, no. 3, Article ID 034203, 2018.
[29] H.-Y. Xing and W. Xu, "The neural networks method for detecting weak signals under chaotic background," *Acta Physica Sinica*, vol. 56, no. 7, pp. 3771–3776, 2007.
[30] H. Lin, L. Yue, and B. Yang, "The neural network method of detecting weak harmonic signal embedded in chaos," *Journal on Communications*, vol. 5, pp. 75–82, 2004.
[31] H.-Y. Xing, Y.-Y. Cheng, and W. Xu, "Detection of weak target signal with least-squares support vector machine and generalized embedding windows under chaotic background," *Acta Physica Sinica*, vol. 61, no. 10, Article ID 100506, 2012.
[32] H. Xing, Z. Qi, and W. Xu, "Weak signal estimation in chaotic clutter using selective support vector machine ensemble," *Acta Physica Sinica*, vol. 61, no. 24, Article ID 240504, 2012.
[33] Z. Lu, Z. Cai, K. Jiang, and C. Li, "Weak signal detection in chaos based on LS-SVM," *Journal of Data Acquisition & Processing*, vol. 23, no. 5, pp. 589–592, 2008.
[34] J.-F. Hu, Y.-X. Zhang, H.-Y. Li, W. Yang, W. Xia, and J. Li, "Harmonic signal detection method from strong chaotic background based on optimal filter," *Acta Physica Sinica*, vol. 64, no. 22, Article ID 220504, 2015.
[35] C. Zheng, Y. Zeng, and Z. Fu, "A novel parameter estimation method of signal in chaotic background," *Acta Physica Sinica*, vol. 1, pp. 46–50, 2008.
[36] H. Li and G. Meng, "Harmoic signal extraction from chaotic interference based on empirical mode decomposition," *Acta Physica Sinica*, vol. 7, pp. 2069–2073, 2004.
[37] F. Wang, J. Guo, Z. Wang et al., "Extraction method of harmonic signals from strong chaotic interference," *Acta Physica Sinica*, vol. 6, pp. 1019–1023, 2001.
[38] L. Su, H. Sun, and C. Li, "LL-P-KF hybrid algorithm for detecting and recovering sinusoidal signal in strong chaotic noise," *Acta Electronica Sinica*, vol. 45, no. 4, pp. 844–854, 2017.
[39] C. Li and L. Su, "Extracting harmonic signal from a chaotic background with local linear model," *Mechanical Systems and Signal Processing*, vol. 84, pp. 499–515, 2017.
[40] F. Takens, "Detecting strange attractors in turbulence," in *Lecture Notes in Mathematics*, vol. 898, pp. 366–381, no. 9, Springer, Berlin, Germany, 1981.
[41] L. Cao, "Practical method for determining the minimum embedding dimension of a scalar time series," *Physica D: Nonlinear Phenomena*, vol. 110, no. 1-2, pp. 43–50, 1997.
[42] C. W. S. Chen and J. C. Lee, "Bayesian inference of threshold autoregressive models," *Journal of Time Series Analysis*, vol. 16, no. 5, pp. 483–492, 1995.
[43] J. Fan and T. Huang, "Profile likelihood inferences on semiparametric varying-coefficient partially linear models," *Bernoulli*, vol. 11, no. 6, pp. 1031–1057, 2005.